

# **Spectroscopy Takes Electrochemistry Beyond the Interface: A Compact Analytical Solution for the Reversible First-Order Catalytic Mechanism**

E. Laborda<sup>a</sup>, J.M. Gómez-Gil<sup>a</sup>, A. Molina<sup>\*,a</sup>, R.G. Compton<sup>b</sup>

<sup>a</sup> *Departamento de Química Física, Facultad de Química, Regional Campus of International Excellence "Campus Mare Nostrum", Universidad de Murcia, 30100 Murcia, Spain*

<sup>b</sup> *Department of Chemistry, Physical & Theoretical Chemistry Laboratory, Oxford University, South Parks Road, Oxford OX1 3QZ, United Kingdom*

\* Corresponding author:

Tel: +34 868 88 7524

Fax: +34 868 88 4148

Email: amolina@um.es

## **Abstract**

The monitoring of the non-interfacial phenomena of mass transport and homogeneous chemical reactions by combining spectroscopic and electrochemical methods is examined. The spectroelectrochemical study of a charge transfer process is addressed, considering the possibilities that the electro-consumed species is regenerated in solution by means of a first-order chemical reaction or that the diffusivity of the oxidized and reduced species differ from each other significantly.

Novel closed-form explicit analytical expressions for the concentration profiles and the absorbance response of all the species for any voltammetric technique are deduced, taking into account the two main working arrangements: the normal-beam and parallel-beam modes. The analytical solutions are particularized to double potential step chronoamperometry and to cyclic voltammetry. The corresponding chronoabsorptometric and voltabsorptometric responses in parallel-mode are proven to provide additional information with respect to electrochemical-only measurements, as well as insights into the solution regions next to the interface where the concentration changes and equilibrium disruptions take place. With this theory the absorptometric response can be related to the physicochemical dynamics of the redox system and to establish optimum configuration and conditions for the study of diffusion and reaction layers, the species diffusion coefficients and the chemical kinetic and equilibrium constants.

**Keywords:** Analytical theory; UV-vis spectroelectrochemistry; Catalytic mechanism; Concentration profiles; Diffusion and Reaction Layers

## 1. Introduction

The complete elucidation and characterization of interfacial charge transfer mechanisms can be challenging when conducted exclusively with electrochemical experiments. With the coupling of spectroscopic techniques, the species involved or affected by the charge transfer during the electrical perturbation can be monitored with the aim of identifying their chemical nature and the reaction pathways [1–5]. Also, the spectroelectrochemical (SEC) signal can provide quantitative information about the mass transport and the (electro)chemical kinetics and thermodynamics on the basis of suitable theoretical treatments [6–10] that describe accurately the concentration profile of the light absorbing species.

In this work, rigorous and closed-form analytical expressions for the concentration profiles of the first-order catalytic mechanism at macroelectrodes are obtained with the Laplace transform method. The solutions are extended to any potential-controlled perturbation (*i.e.*, any voltammetric technique) and they are easy to integrate and implement given their compact form. As a result, simple closed-form analytical expressions are deduced for the absorptometric response in both the normal-beam ( $A_N$ ) and parallel-beam ( $A_P$ ) configurations.

The case of simple charge transfers (the E mechanism) is also considered, reporting analytical expressions for  $A_N$  and  $A_P$  in any multi-pulse technique and taking into account that the diffusivity of the oxidized and reduced species can differ notably in some systems such as electron transfers in room temperature ionic liquids [11], ion transfers between conventional solvents and liquid membranes [12], and the oxidative or reductive dissolution of nanoparticles.

The theory is employed to examine critically the value of spectroelectrochemical measurements in the determination of the catalytic kinetic and equilibrium constants, as well as of the diffusion coefficients of the oxidized and reduced species with a single experiment. The cyclic voltammetry and double potential pulse chronoamperometry techniques are considered, comparing the sensitivity of the electrochemical response with that of the normal-mode and

parallel-mode absorptometries. This enables us to establish the optimum configuration and operational conditions for quantitative analyses.

The study of the so-called diffusion and reaction layers via spectroelectrochemical experiments in parallel-beam configuration is shown to be particularly useful. Accurate and simple expressions and protocols are derived to relate the  $A_p$ -value at different distances from the interface with the concentration profile of the photoactive species [13]. It is important to highlight that reproducing the profile of the light absorbing species is of great interest to analyse the incidence of thin-layer diffusion, convergent diffusion, convective mass transport and of the electrical double layer [14]. Also, it can be useful for imaging the electrochemical activity over the interface as well as for monitoring its conditions (*eg.*, interfacial pH) and geometry.

## 2. Glossary:

$A_{i,N}^{[m]}(t)$  UV-visible absorbance response of species  $i$  ( $i \equiv O, R$ ) at the  $m$ -th potential pulse applied ( $m = 1, 2, \dots$ ) considering normal incidence of the light beam.

$A_{i,P}^{[m]}(t)$  UV-visible absorbance response of species  $i$  ( $i \equiv O, R$ ) at the  $m$ -th potential pulse applied ( $m = 1, 2, \dots$ ) in the parallel working arrangement.

$A_{R,P}^*$  Normalized UV-visible absorbance response of species  $i$  ( $i \equiv O, R$ ) considering the parallel working arrangement.

$c_i^{[m]}(x, t)$  Concentration profile of species  $i$  ( $i \equiv O, R$ ) at the  $m$ -th potential pulse applied.

$c_i^{[m],\text{sup}}$  Surface concentration of species  $i$  ( $i \equiv O, R$ ) at the  $m$ -th potential pulse applied.

$c_i^*$  Bulk concentration of species  $i$  ( $i \equiv O, R$ ).

$c_T$  Total concentration of electroactive species ( $= c_O + c_R$ ).

$D$  Diffusion coefficient of the electroactive species when equal diffusivities are considered.

$D_i$  Diffusion coefficient of species  $i$  ( $i \equiv O, R$ ).

$\delta_{i,d}^{\text{lin}}$  Thickness of the linear diffusion layer for species  $i$ .

$\delta_{i,d}^{\text{real}}$  Thickness of the real diffusion layer for species  $i$ .

$\delta_r^{\text{lin}}$  Thickness of the linear reaction layer.

$\delta_r^{\text{SS,lin}}$  Thickness of the linear reaction layer under steady-state conditions.

$\delta_r^{\text{real}}$  Thickness of the real reaction layer.

$E^{[m]}$   $m$ -th potential pulse applied.

$E^0$  Formal potential of the redox couple O/R.

$E_{1/2}$  Half-wave potential.

$\Delta E$  Step potential of the staircase perturbation in cyclic voltammetry.

$E_{\text{init}}$  Initial potential applied in a cyclic waveform perturbation.

$E_{\text{fin}}$  Last potential applied during the forward scan in cyclic voltammetry.

$\varepsilon_i$  Extinction coefficient of species  $i$  ( $i \equiv O, R$ ).

$\phi^{[m]}$  Variable related to the perturbation of the chemical equilibrium (in this case a catalytic chemical reaction) at the  $m$ -th potential pulse applied.

$\bar{\phi}^{[m]}$  Laplace transform of the  $\phi^{[m]}$ -function at the  $m$ -th potential pulse applied.

$\gamma$  Square root of the ratio between the diffusion coefficient of species O and R.

$i$  Index for electroactive species ( $i \equiv \text{O}, \text{R}$ ).

$K$  Chemical equilibrium constant of the reversible catalytic mechanism.

$k_1$  Kinetic constant of the chemical conversion of species R to O.

$k_2$  Kinetic constant of the chemical conversion of species O to R.

$\kappa$  Sum of the chemical kinetics equilibrium constants of a reversible (pseudo)first order catalytic mechanism ( $= k_1 + k_2$ ).

$L$  Laplace transform operator.  $L^{-1}$  Laplace antitransform operator.

$L$  Path length of the beam through the material sample in the *normal-beam mode*.

$L_e$  Path length of the beam over the electrode surface in the *parallel-beam configuration*.

$N$  Total number of pulses applied during a cyclic voltammetry waveform perturbation.

$\nu$  Scan rate of the cyclic voltammetry.

$w$  Width of the light beam in the *parallel configuration*.

$x_0$  Distance closer to the electrode surface of the incidence of the light beam in the parallel-arrangement.



$$\eta_1 = \frac{F}{RT}(E_1 - E^0) \quad (2)$$

and F, R and T have their usual meaning. Note that in the bvp (1) it is assumed that the electroactive species show equal diffusion coefficients ( $D$ ) and that the electron transfer is reversible.

For the resolution of the above problem, it is convenient to introduce the following variables:

$$\left. \begin{aligned} c_T^{[1]}(x,t) &= c_O^{[1]}(x,t) + c_R^{[1]}(x,t) \\ \phi^{[1]}(x,t) &= c_R^{[1]}(x,t) - K c_O^{[1]}(x,t) \end{aligned} \right\} \quad (3)$$

where  $c_T^{[1]}(x,t)$  is the total concentration of electroactive species at a certain point in solution and any time of the experiment, and  $\phi^{[1]}(x,t)$  accounts for the extent of the perturbation of the chemical equilibrium: the greater the equilibrium disruption, the larger the  $\phi^{[1]}$ -value.

It can be easily demonstrated that the total concentration  $c_T^{[1]}(x,t)$  remains constant at any point of the solution and time of the experiment in the catalytic mechanism described by Eqs.(1) [15,16]:

$$c_T^{[1]}(x,t) = c_O^{[1]}(x,t) + c_R^{[1]}(x,t) = c_O^* + c_R^* = c_T \quad \forall (x,t) \quad (4)$$

which enables us to reduce (1) to the following single-variable problem:

$$\left. \begin{aligned} \frac{\partial \phi^{[1]}(x,t)}{\partial t} &= D \left( \frac{\partial^2 \phi^{[1]}(x,t)}{\partial x^2} \right) - \kappa \phi^{[1]} & (a) \\ \left. \begin{aligned} t &= 0, x \geq 0 \\ t &> 0, x \rightarrow \infty \end{aligned} \right\} &\rightarrow \phi^{[1]}(x,t) = 0 & (b) \\ t > 0, x = 0 &\rightarrow \phi^{[1]}(0) = c_T \frac{1 - Ke^{\eta_1}}{1 + e^{\eta_1}} & (c) \end{aligned} \right\} \quad (5)$$

with

$$\kappa = k_1 + k_2 \quad (6)$$



To solve the differential equation problem (5), the Laplace transform method is employed, according to which the differential equation becomes into:

$$\left( \frac{d^2 \bar{\phi}^{[1]}(x, s)}{dx^2} \right) - \left( \frac{s + \kappa}{D} \right) \bar{\phi}^{[1]} = 0 \quad (7)$$

which has the following solution considering the boundary conditions:

$$\bar{\phi}^{[1]}(x, s) = \bar{\phi}^{[1]}(0, s) e^{\left( -x \sqrt{\frac{s + \kappa}{D}} \right)} \quad (8)$$

Applying the inverse transform, the solution for the variable  $\phi(x, t)$  is:

$$\begin{aligned} \phi^{[1]}(x, t) &= \mathcal{L}^{-1} \left[ \bar{\phi}^{[1]}(x, s) \right] = \left\{ \phi^{[1]}(0) \cdot \mathcal{L}^{-1} \left[ \frac{1}{s} e^{-x \sqrt{\frac{s + \kappa}{D}}} \right] \right\} = \\ &= \phi^{[1]}(0) \frac{1}{2} \left[ e^{\left( -x \sqrt{\frac{\kappa}{D}} \right)} \operatorname{erfc} \left( \frac{x}{2\sqrt{Dt}} - \sqrt{\kappa t} \right) + e^{\left( x \sqrt{\frac{\kappa}{D}} \right)} \operatorname{erfc} \left( \frac{x}{2\sqrt{Dt}} + \sqrt{\kappa t} \right) \right] \end{aligned} \quad (9)$$

where  $\phi^{[1]}(0)$  is defined in Eq. (5c). The expressions of the concentration profiles of species O and R are immediately obtained from Eqs. (3) and (4):

$$\begin{aligned} c_O^{[1]}(x, t) &= \frac{c_T}{1 + K} \left\{ 1 + \frac{1 - K e^{\eta}}{1 + e^{\eta}} f_{\text{Cat}}(x, t) \right\} \\ c_R^{[1]}(x, t) &= c_T - c_O^{[1]}(x, t) \end{aligned} \quad (10)$$

with

$$f_{\text{Cat}}(x, t) = \frac{1}{2} \left[ e^{\left( -x \sqrt{\frac{\kappa}{D}} \right)} \operatorname{erfc} \left( \frac{x}{2\sqrt{Dt}} - \sqrt{\kappa t} \right) + e^{\left( x \sqrt{\frac{\kappa}{D}} \right)} \operatorname{erfc} \left( \frac{x}{2\sqrt{Dt}} + \sqrt{\kappa t} \right) \right] \quad (11)$$

The concentration profiles given by Eqs. (10)-(11) are valid for any value of the chemical equilibrium constant (K) and chemical kinetics ( $\kappa$ ) and they coincide with those obtained previously for the particular case of an irreversible chemical catalysis (K=0) [17,18]. The

expressions of the surface concentrations can also be derived from Eqs. (10)–(11) by making  $x=0$ :

$$\left. \begin{aligned} c_{\text{O}}^{[1],\text{Cat},\text{sup}} &\equiv c_{\text{O}}^{[1],\text{Cat}}(0) = \frac{c_{\text{T}}}{1+K} \frac{e^{\eta_1}}{1+e^{\eta_1}} \\ c_{\text{R}}^{[1],\text{Cat},\text{sup}} &\equiv c_{\text{R}}^{[1],\text{Cat}}(0) = c_{\text{T}} \frac{K}{1+K} \frac{e^{\eta_1}}{1+e^{\eta_1}} \end{aligned} \right\} \quad (12)$$

which are equivalent to those previously obtained [16](see also Eqs. (3)–(4) and (5c)).

Note that the introduction of the variable  $\phi(x, t)$  greatly simplifies the resolution of the problem by the Laplace transform method and it enables closed-form expressions to be obtained for the concentration profiles which are easier to implement and integrate than previous series solutions [15,16].

### 3.1.2. *Multipulse techniques*

Let us consider now the application of an arbitrary sequence of potential pulses  $(E^{[1]}, E^{[2]}, \dots, E^{[m]})$  of the same time length ( $\tau$ ). Considering that the diffusive operator is linear, then it is possible to write that (see [19]):

$$\phi^{[m]}(x, t) = \phi^{[m-1]} + \tilde{\phi}^{[m]} = \phi^{[1]}(x, m\tau) + \sum_{j=2}^m \tilde{\phi}^{[j]}(x, (m-j+1)\tau) \quad (13)$$

where  $\tilde{\phi}^{[m]}$  corresponds to the *unknown partial solution* of the problem corresponding to the  $m$ -th potential pulse and  $\phi^{[1]}$  is given in Eq.(9).

Following a mathematical procedure equivalent to that employed in [19], the problem for each potential pulse applied can be written as a function of only the *unknown partial solution*  $\tilde{\phi}^{[m]}$ , which is formally equivalent to that for a single potential pulse (Eqs. (5)) and it has the following solution [19]:

$$\tilde{\phi}^{[m]}(x, t) = \zeta^* \left( \frac{1 - Ke^{\eta_m}}{1 + e^{\eta_m}} - \frac{1 - Ke^{\eta_{m-1}}}{1 + e^{\eta_{m-1}}} \right) f_{\text{Cat}}(x, (m-j+1)\tau); \quad m > 1 \quad (14)$$

where  $f_{\text{Cat}}(x, (m-j+1)\tau)$  is given by Eq.(11) with:  $t = (m-j+1)\tau$ .

The expression for  $\phi^{[m]}(x, t)$  at the  $m$ -th potential pulse can be obtained from Eq.(13), considering that  $\phi^{[1]}(0)$  is defined in Eqs. (5c) and (14). Then, attending to Eq. (3) and that the total concentration remains constant:

$$c_T = c_O^{[m]}(x, t) + c_R^{[m]}(x, t); \quad \forall (x, t) \quad (15)$$

the concentration profiles of species O and R are deduced:

$$c_O^{[m], \text{Cat}}(x, t) = \frac{c_T}{1+K} \left[ \left( 1 - \frac{1 - Ke^{\eta_l}}{1 + e^{\eta_l}} f_{\text{Cat}}(x, m\tau) \right) - \sum_{j=2}^m \left( \frac{1 - Ke^{\eta_j}}{1 + e^{\eta_j}} - \frac{1 - Ke^{\eta_{j-1}}}{1 + e^{\eta_{j-1}}} \right) f_{\text{Cat}}(x, (m-j+1)\tau) \right] \quad (16)$$

as well as the surface concentrations at any  $m$ -th potential pulse:

$$c_O^{[m], \text{Cat-surf}} \equiv c_O^{[m], \text{Cat}}(0) = \frac{c_T}{1+K} \frac{e^{\eta_m}}{1 + e^{\eta_m}} \quad (17)$$

Note that the equivalent expressions for species R can be obtained from those of the oxidized species (Eqs. (16) or (17)) attending to the relationship given by Eq.(15).

### 3.2. Simple charge transfer: the E mechanism

The concentration profiles for the E mechanism when the diffusion coefficients of the oxidized and reduced species are the same can be directly obtained from Eqs. (11) and (16) by making  $(\kappa \rightarrow 0)$  with the ratio  $c_B^*/c_C^*$  corresponding to the ratio between the bulk concentrations:

$$\left. \begin{aligned} c_O^{[m], \kappa \rightarrow 0}(x, t) &= c_O^* \left[ \left( 1 - \frac{1}{1 + e^{\eta_l}} \operatorname{erfc} \left( \frac{x}{2\sqrt{Dm\tau}} \right) \right) - \sum_{j=2}^m \left( \frac{1}{1 + e^{\eta_j}} - \frac{1}{1 + e^{\eta_{j-1}}} \right) \operatorname{erfc} \left( \frac{x}{2\sqrt{D(m-j+1)\tau}} \right) \right] \\ c_R^{[m], \kappa \rightarrow 0} &= (c_O^* + c_R^*) - c_O^{[m], \kappa \rightarrow 0} \end{aligned} \right\} \quad (18)$$

#### 4. Results and Discussion:

##### 4.1. Simple charge transfer with different diffusivities when species R is not initially present

First, the value of the coupling of spectroscopic and electrochemical techniques will be analyzed with respect to the study of reversible charge transfers, considering the most common situation where only the reagent species is initially present (i.e.:  $c_R^* = 0$ ). Under conditions where significant differences between the diffusion coefficients arise, the superposition principle is also applicable in the case of macroelectrodes [16,17,20] and the following expression is obtained for the concentration profiles in any single or multipulse technique:

$$\left. \begin{aligned} c_O^{[m],E}(x,t) &= c_O^* \left[ 1 - Z_1^E \operatorname{erfc} \left( \frac{x}{2\sqrt{D_O m \tau}} \right) - \sum_{j=2}^m Z_j^E \operatorname{erfc} \left( \frac{x}{2\sqrt{D_O (m-j+1) \tau}} \right) \right] \\ c_R^{[m],E}(x,t) &= \gamma c_O^* \left[ Z_1^E \operatorname{erfc} \left( \frac{x}{2\sqrt{D_R m \tau}} \right) + \sum_{j=2}^m Z_j^E \operatorname{erfc} \left( \frac{x}{2\sqrt{D_R (m-j+1) \tau}} \right) \right] \end{aligned} \right\} \quad (19)$$

with  $\gamma = \sqrt{D_O / D_R}$  and:

$$\left. \begin{aligned} Z_1^E &= \frac{1}{1 + \gamma e^{\eta_1}} \\ Z_j^E &= \frac{1}{1 + \gamma e^{\eta_j}} - \frac{1}{1 + \gamma e^{\eta_{j-1}}}; \quad j = 2, 3, \dots \end{aligned} \right\} \quad (20)$$

with:

$$\eta_j = \frac{F}{RT} (E_j - E^{0'}) ; \quad j = 1, 2, \dots, m \quad (21)$$

##### 4.1.1. Normal-beam mode

The absorbance response in the normal-beam configuration for species  $i$  at a certain  $m$ -th potential pulse is given by [1,6]:

$$A_{i,N}^{[m]}(t) = \varepsilon_i \int_0^L c_i^{[m]} dx \quad ; \quad m = 1, 2, \dots \quad (22)$$

with  $L$  being the optical path length (cell length),  $\varepsilon_i$  the molar extinction coefficient of species  $i$  and  $c_i^{[m]}$  the concentration profile of the corresponding species  $i$  (O or R) at the  $m$ -th potential pulse given by Eqs. (19). Note that in the case of UV-vis spectroscopy, it is implicitly assumed that the Beer-Lambert Law applies so that absorbance scales linearly with concentration. Thus, the absorbance response of the electrogenerated reduced species can be calculated from:

$$A_{R,N}^{[m],E}(t) = \varepsilon_R c_O^* \left( 2\sqrt{\frac{D_O}{\pi}} \right) \left( Z_1^E \sqrt{m\tau} + \frac{1}{\gamma} \sum_{j=2}^m Z_j^E \sqrt{(m-j+1)\tau} \right) \quad (23)$$

with  $Z_1^E$  and  $Z_j^E$  being given in Eq.(20).

Note that Eq.(23) is directly related with the converted charge in the E-mechanism (see [1]) and, the sum of the normalized absorbance of species O and R at a given time of the experiment, independently of the value of the diffusion coefficients, fulfils that:

$$1 = \frac{A_{O,N}^{[m],E}}{\varepsilon_O L c_O^*} + \frac{A_{R,N}^{[m],E}}{\varepsilon_R L c_O^*} \quad (24)$$

so that the absorbance corresponding to species O can be easily calculated from Eqs.(23)-(24).

Considering the double potential chronoamperometry (DPC) under limiting current conditions, the chronoabsorptometric response of species R is obtained from Eq.(23) by making  $e^{\eta_1} \rightarrow 0$  and  $e^{\eta_2} \rightarrow \infty$  [1,7]:

$$\left. \begin{aligned} \frac{A_{R,N}^{[1],E-Lim}(t_1)}{\varepsilon_R c_O^*} &= 2\sqrt{\frac{D_O}{\pi}} \sqrt{t_1}; & 0 < t_1 \leq \tau \\ \frac{A_{R,N}^{[2],E-Lim}(\tau + t_2)}{\varepsilon_R c_O^*} &= 2\sqrt{\frac{D_O}{\pi}} \left( \sqrt{(\tau + t_2)} - \sqrt{t_2} \right); & 0 < t_2 \leq \tau \end{aligned} \right\} \quad (25)$$

which coincide with the expressions reported [6,7]. From Eqs.(25), it can be deduced that neither  $A_{R,N}^{[1],E-Lim}$  nor  $A_{R,N}^{[2],E-Lim}$  are sensitive to the diffusivity of species R when this is not initially present in solution, similarly to the behaviour observed for the current responses ([1]

and  $I^{(2)}$  [16,21]. Hence, the simultaneous determination of  $D_O$  and  $D_R$  is not feasible as shown in

Figure 1.A.

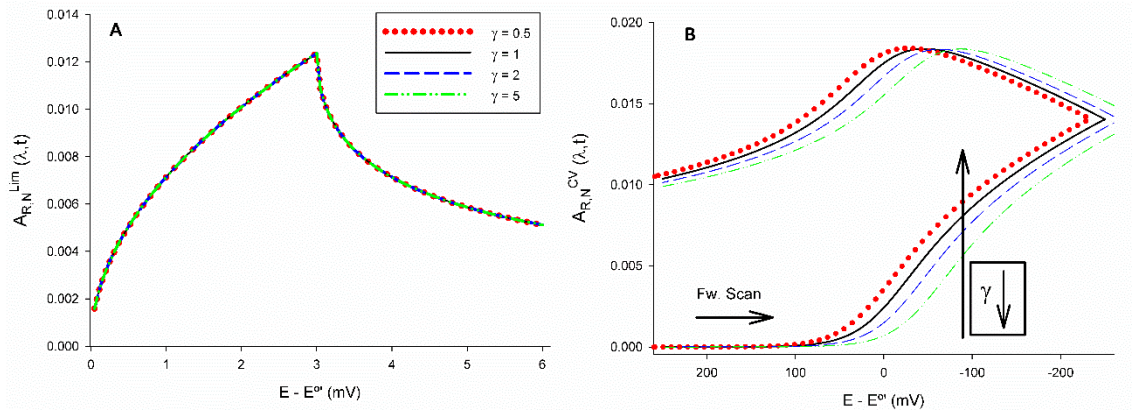


**Figure 1.** Influence of the diffusion coefficient of the reduced species ( $D_R$ ) on **A**) the theoretical double potential chronoabsorptometric response under limiting current conditions (Eq.(25)) and **B**) on the theoretical cyclic voltabsorptometric response of species R (Eqs. (21), (23), (26) and (27),  $v=0.1Vs^{-1}$  and  $|\Delta E| = 0.01mV$ ). Other conditions:  $D_O=10^{-5} cm^2s^{-1}$ ,  $c_O^* = 10^{-3} M$ ,  $\epsilon_R=2 \cdot 10^3 M^{-1}cm^{-1}$ ,  $L=1cm$  and  $T=298K$ .

The absorptometric response in cyclic voltammetry (CV) can be calculated from Eq.(23) considering a staircase-like potential perturbation with a very small step amplitude ( $\Delta E$ )  $\leq 0.01$  mV [16,22], so that:

$$(m-j+1)\tau = \begin{cases} = \frac{|E^{[m-j+1]} - E_{init}|}{v}; & j \leq N/2 \\ = \frac{|2E_{fin} - E^{[m-j+1]} - E_{init}|}{v}; & j > N/2 \end{cases} \quad (26)$$

and in Eq.(21):

$$E_j \begin{cases} = E_{init} - j\Delta E; & j = 1, 2, \dots (N/2) \\ = E_{fin} + j\Delta E; & j > (N/2) \end{cases} \quad (27)$$

with  $N$  being the total number of pulses applied in the cyclic scan,  $E_{init}$  and  $E_{fin}$  the initial and final values of the forward scan, respectively, and  $v$  the scan rate ( $v=dE/dt$ ).

With regard to the cyclic voltabsorptograms (Fig. 1.B), they shift towards more negative potentials as the diffusivity of the species R decreases according with the variation of the half-wave potential:  $E_{1/2} = E^{0'} - \frac{RT}{F} \ln(\gamma)$ , and with the effect observed in the cyclic voltammograms.

Note that the above results point out that the normal absorptometric response has similar limitations to those of the electrochemical response for the simultaneous determination of diffusion coefficients, that is, the response in DPC is insensitive while the signal in CV shows low sensitivity and accurate values of  $E^{0'}$  are required.

#### 4.1.2. *Parallel-beam mode:*

In the parallel-beam configuration, the absorptometric response of species  $i$  is calculated as [8,9,23]:

$$A_{i,P}^{[m]}(t) = \log \left( \frac{w}{\int_{x_0}^{x_0+w} 10^{-\varepsilon_i L_e c_i^{[m]}(x,t)} dx} \right) \quad (28)$$

with  $x_0$  being the distance closer to the electrode surface,  $w$  the width of the light beam,  $L_e$  the optical path length and  $c_i^{[m]}$  the concentration profile of the light absorbing species  $i$  (Eqs. (19) ).

The value of the spectroelectrochemical measurements in the parallel-beam mode with a moving slit to examine the depletion layer of a simple electron- or ion-transfer (the E mechanism) is studied in Figure 2 for a double potential step chronoamperometric experiment [13]. The concentration profile is very sensitive to  $\gamma (= \sqrt{D_O/D_R})$  and it shows a maximum (Fig.2.B) in the second potential pulse, contrarily to the monotonous decrease towards the bulk solution during the first pulse (Fig.2.A, see also Eqs. (19) and (20)). It can be seen that the parallel-beam curves reflect satisfactorily these features of the photoactive species profile in both, the first and second potential pulses, provided that a small enough beam width is employed ( $w/\sqrt{\pi D_i t} < 1.7$  for  $\gamma=2$  in Figure 2.A). Otherwise (see  $\gamma=2$  in Fig.2.B), the parallel-beam curves show some disagreement with respect to the real concentration profiles since the

diffusion layer takes place in a narrow region (ca.  $\approx 60\mu\text{m}$ ) that cannot be resolved adequately with  $w=30\mu\text{m}$ .

The above procedure allow us to get direct access to the *real* diffusion layer ( $\delta_{i,d}^{\text{real}}$ ). As can be seen in Figure 2, the thickness of the region perturbed by the electrode reaction differs greatly from the *linear* diffusion layer ( $\delta_{i,d}^{\text{lin}} = \sqrt{\pi D_i t}$ , indicated on the graphs in Fig. **2.A** and **2.C**) that is the magnitude accessible via electrochemical-only studies (e.g.: for  $\gamma=2$  and  $t=1\text{s}$ ,  $\delta_{R,d}^{\text{real}} = 58\mu\text{m} > \delta_{R,d}^{\text{lin}} = 28\mu\text{m}$ ) [24,25].

From this Figure, it is clear that the  $A_{R,P}^E$ -signal when a narrow width-beam is employed ( $w/\sqrt{\pi D_i t} \leq 1.25$  for  $0.5 < \gamma < 2$ , see Section S.I of the Supp. Info.) is well described by:

$$\left. \begin{aligned} A_{R,P}^{[1],E}(x_0, t_1) &\approx \varepsilon_R L_e c_O^* \gamma Z_1^E \operatorname{erfc}\left(\frac{x_0 + w/2}{2\sqrt{D_R t_1}}\right) \\ A_{R,P}^{[2],E}(x_0, \tau_1 + t_2) &\approx \varepsilon_R L_e c_O^* \gamma \left\{ Z_1^E \operatorname{erfc}\left(\frac{x_0 + w/2}{2\sqrt{D_R (\tau_1 + t_2)}}\right) + Z_2^E \operatorname{erfc}\left(\frac{x_0 + w/2}{2\sqrt{D_R t_2}}\right) \right\} \end{aligned} \right\} \quad (29)$$

with  $Z_1^E$  and  $Z_2^E$  being given by Eq.(20). Also, note that by using a model charge transfer process (i.e., with well-known  $\varepsilon_R, L_e, c_O^*$  and  $D_R$ -values), Eq.(29) can be used to determine the position of the light-beam, that is, the  $x_0$ -value.

The above expressions can be extended to any multipulse technique (not shown) such that:

$$\left. \begin{aligned} A_{O,P}^{[m],E}(x_0, t) &\approx \varepsilon_O L_e c_O^* \left[ 1 - Z_1^E \operatorname{erfc}\left(\frac{x_0 + w/2}{2\sqrt{D_O (\tau_1 + t_2)}}\right) - \sum_{j=2}^m Z_j^E \operatorname{erfc}\left(\frac{x_0 + w/2}{2\sqrt{D_O (m-j+1)\tau}}\right) \right] \\ A_{R,P}^{[m],E}(x_0, t) &\approx \varepsilon_R L_e c_O^* \gamma \left[ Z_1^E \operatorname{erfc}\left(\frac{x_0 + w/2}{2\sqrt{D_R (\tau_1 + t_2)}}\right) + \sum_{j=2}^m Z_j^E \operatorname{erfc}\left(\frac{x_0 + w/2}{2\sqrt{D_R (m-j+1)\tau}}\right) \right] \end{aligned} \right\} \quad m = 1, 2, \dots \quad (30)$$

with  $Z_1^E$  and  $Z_j^E$  being given by Eq.(20).



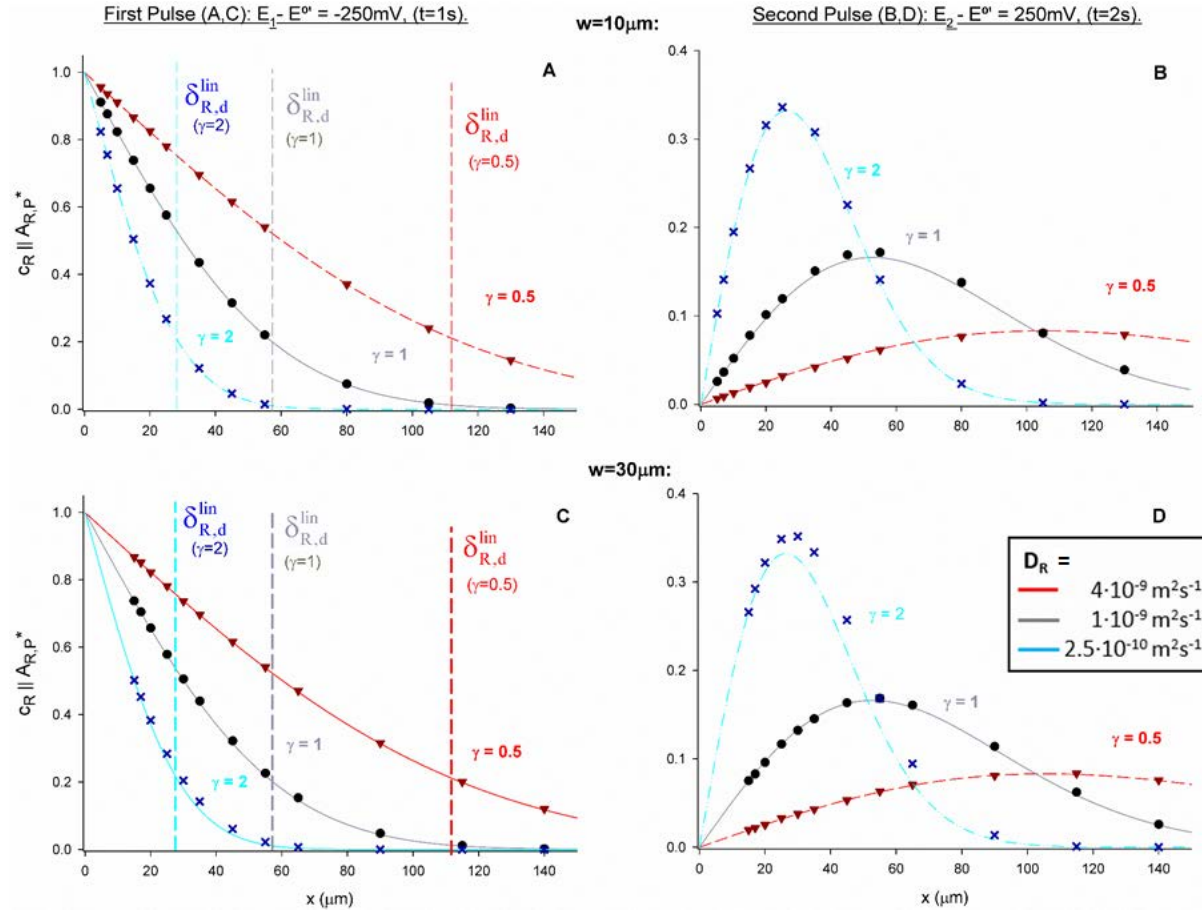


**Figure 2.** Influence of the  $D_R$ -value on the theoretical normalized parallel-beam absorptometric response of species R (points,  $A_{R,P}^* = A_{R,P}^*/(\epsilon_R L_e)$ ) at the end of the first (A, C) and second (B, D) chronoamperograms when a moving parallel-beam of 10  $\mu\text{m}$  (A, B) or 30  $\mu\text{m}$  (C, D) width and an optical length of 0.4 cm ( $L_e$ ) is employed (Eqs. (19) - (21) and (28)). Solid lines corresponds to the theoretical concentration profile of species R (Eqs. (19) - (21)) and dashed lines indicate the thickness of the linear diffusion layer of species R ( $\delta_{R,d}^{lin} = \sqrt{\pi D_R t}$ ) at the end of the first pulse (A, C). Other conditions as in Figure 1.

Next, the value of the parallel-beam response for the determination of the diffusion coefficient of the electrogenerated species will be examined. In Figure 3, the influence of the diffusivity of species R ( $D_R$ ) on the DPC-chronoabsorptometric (Fig. 3.A) and on the cyclic voltabsorptometric (Fig. 3.B) responses is shown for  $w=10\text{ }\mu\text{m}$ . As can be seen, the DPC-chronoabsorptogram and the cyclic voltabsorptogram are very sensitive to the  $D_R$ -value (see Figs. 3.A and 3.B), with the signal increasing as the  $D_R$ -value becomes smaller due to larger accumulation of photoactive species near the electrode surface.

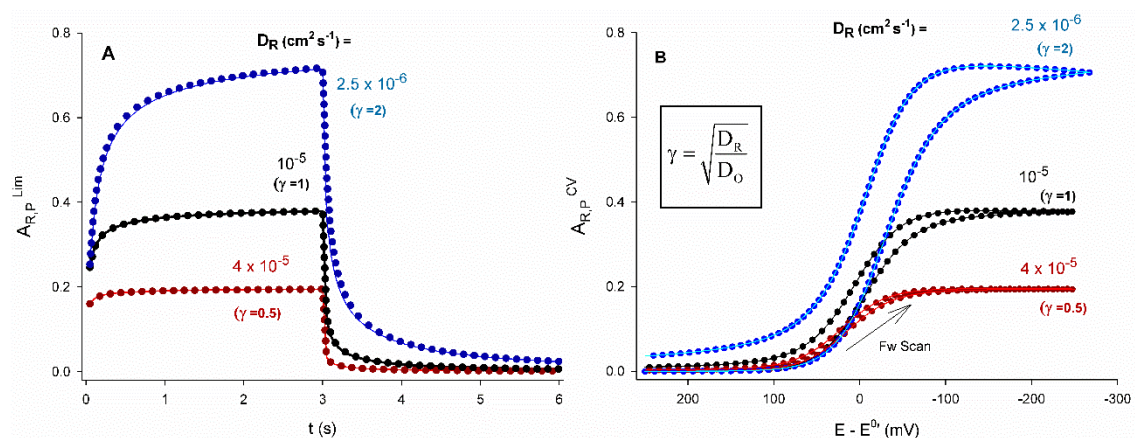


**Figure 3.** Influence of the diffusion coefficient of the reduced species ( $D_R$ ) **A)** on the double potential chronoabsorptometric (Eqs. (19) - (21) and (28), solid lines), and **B)** on the cyclic voltabsorptometric (Eqs. (19) - (21) and (26) - (28), solid lines) theoretical responses of species R in the parallel-beam arrangement ( $w=10\mu\text{m}$ ,  $L_e=0.4\text{cm}$ ). Dotted lines (points) corresponds to the theoretical absorptometric response obtained from Eqs.(29) or (30). Other conditions as in Figure 1.

The satisfactory agreement between the results obtained with Eq.(28) and the closed-form expressions (29) - (30) points out that the latter describe accurately the parallel-beam SEC signal in a simple and rapid way when a narrow beam width is employed. Note that this implies that, under such conditions, the parallel-beam absorbance can be taken as the absorbance of the *infinitesimally*-thin solution layer located at the centre of the light beam ( $x_0+w/2$ ) with little error (see Section S.I of the Supp. Info.).

## 4.2. Reversible (pseudo)first-order catalytic mechanism

In this section, the study of a (pseudo-)first order catalytic mechanism via spectroelectrochemical methods is considered, paying special attention to the determination of the catalytic rate constants and to the study of the region where the chemical equilibrium is perturbed: the so-called reaction layer [24,25].

### 4.2.1. Normal-beam mode

The absorbance in normal-beam mode is easily determined by inserting Eqs. (11) and (16) in Eq. (22):

$$\left. \begin{aligned} A_{O,N}^{[m],Cat}(t) &= \frac{\varepsilon_O C_T}{1+K} \left[ L - Z_1^{Cat} F(m\tau) - \sum_{j=2}^m Z_j^{Cat} F((m-j+1)\tau) \right] \\ A_{R,N}^{[m],Cat}(t) &= \frac{\varepsilon_R C_T}{1+K} \left[ KL + Z_1^{Cat} F(m\tau) + \sum_{j=2}^m Z_j^{Cat} F((m-j+1)\tau) \right] \end{aligned} \right\} \quad (31)$$

with  $Z_1^{Cat}$  and  $Z_j^{Cat}$  :

$$\begin{aligned} Z_1^{Cat} &= \frac{1 - Ke^{\eta_1}}{1 + e^{\eta_1}} \\ Z_j^{Cat} &= \frac{1 - Ke^{\eta_j}}{1 + e^{\eta_j}} - \frac{1 - Ke^{\eta_{j-1}}}{1 + e^{\eta_{j-1}}}; \quad j = 2, 3, \dots \end{aligned} \quad (32)$$

and  $F(t)$  being the integrated function of Eq.(11) from  $x=0$  to  $x=L$  (see also Eq.(22)):

$$F(t) = \sqrt{\frac{D}{\kappa}} \operatorname{erf} \sqrt{\kappa t} \quad (33)$$

For sufficiently fast catalytic kinetics ( $\sqrt{\kappa t} > 2$ , [15]),  $F(t) \rightarrow \sqrt{\frac{D}{\kappa}}$  (i.e.,  $\operatorname{erf}(\sqrt{\kappa t}) \approx 1$ ), a true

steady-state response is reached (even at macroelectrodes) and Eq.(15) greatly simplifies to:

$$A_{R,N}^{SS,Cat} = \frac{\varepsilon_R C_T}{1+K} \left( KL + \frac{1 - Ke^{\eta}}{1 + e^{\eta}} \sqrt{\frac{D}{\kappa}} \right) \quad (34)$$

Note that the following relationship is fulfilled between the normal absorptometric responses for any potential perturbation applied since Eq.(4) is satisfied:

$$1 = \frac{A_{O,N}^{[m],Cat}}{\varepsilon_O L c_T} + \frac{A_{R,N}^{[m],Cat}}{\varepsilon_R L c_T}; m = 1, 2, \dots \quad (35)$$

In the particular case of the DPC-technique under limiting current conditions, the chronoabsorptometric response in the first and second potential pulse are given by:

$$\left. \begin{aligned} A_{R,N}^{[1],Cat-Lim} &= \frac{\varepsilon_R c_T}{1 + K_{cat}} \left( KL + \sqrt{\frac{D}{\kappa}} \operatorname{erf} \sqrt{\kappa t} \right) \\ A_{R,N}^{[2],Cat-Lim} &= \frac{\varepsilon_R c_T}{1 + K_{cat}} \left[ KL + \sqrt{\frac{D}{\kappa}} \left( \operatorname{erf} \sqrt{\kappa (\tau_1 + t_2)} - (1 + K) \operatorname{erf} \sqrt{\kappa t_2} \right) \right] \end{aligned} \right\} \quad (36)$$

which reproduce those obtained previously for the particular case of an irreversible catalytic reaction ( $K=0$ ) [7]. Note that the expressions for the oxidized species,  $A_{O,N}^{[1],Cat-Lim}$  and  $A_{O,N}^{[2],Cat-Lim}$ , are immediately obtained from Eqs.(35) and (36).

From Eqs. (31)-(34) and (36), it can be inferred that the term  $KL$  will prevail for reversible catalytic reactions ( $K \neq 0$ ) and it will mask the kinetic influence ( $L \gg \sqrt{\frac{D}{\kappa}}$ ). Thus, significant effects of the catalytic kinetics on the normal-beam signal are only expected when the chemical reaction is irreversible as shown in Fig. 4. In this figure, it can be seen that the faster the chemical kinetics is, the smaller the absorptometric signal of the reduced species becomes since  $R$  is chemically consumed faster (as predicted by Eqs.(31)-(36)). Also, similarly to the current response, the chronoabsorptometric and cyclic voltabsorptometric responses evolve from a transient to a stationary regime as  $\kappa$  increases (see Eqs.(31)-(34)). Thus, the chronoabsorptograms tend to a time-independent value (Fig. 4.A, green line) while the voltabsorptometric signal tends to a sigmoidal shape where the forward and backward scans (almost) overlap (green line, Fig.4.B).

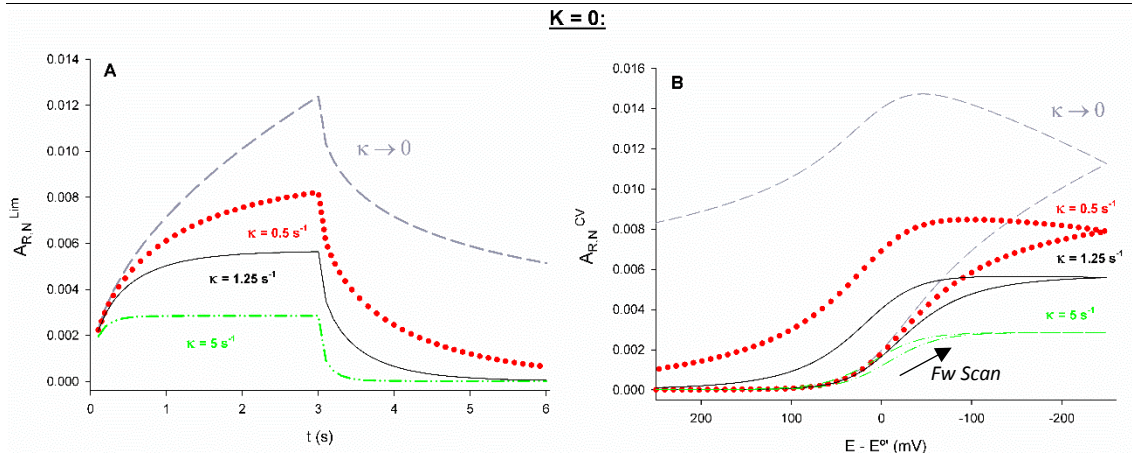


**Figure 4.** Influence of the chemical kinetic constants ( $\kappa$ ) on the double potential step chronoabsorptometric under limiting current conditions **(A)** and cyclic voltabsorptometric **(B)** theoretical responses of species R in the normal-beam arrangement for an irreversible catalytic reaction. The chronoabsorptometric responses were obtained with Eq.(36) and the cyclic voltabsorptograms with Eqs.(26), (27) and (31) - (33). Other conditions as in Figure 3.

For the estimation of the chemical kinetic constants for an irreversible catalytic reaction ( $K=0$ ), the value of  $\kappa$  can be obtained for  $\sqrt{\kappa t} < 2$  from the ratio of the absorbance measured at the end of the first potential step (i.e.,  $t=\tau$ ) and at  $t=2\tau$  (for the duration of both pulses being the same) [7] (see Eqs.(36)):

$$\left| \frac{A_{R,N}^{[2],\text{Cat-Lim}}(2\tau) - A_{R,N}^{[1],\text{Cat-Lim}}(\tau)}{A_{R,N}^{[1],\text{Cat-Lim}}(\tau)} \right| = 2 - \frac{\text{erf}(\sqrt{2\kappa\tau})}{\text{erf}(\sqrt{\kappa\tau})} \quad (37)$$

For  $\sqrt{\kappa t} > 2$ ,  $\kappa$  can be determined directly from the absorbance at the end of the first potential pulse:

$$A_{R,N}^{\text{SS},K=0} = \varepsilon_R c_T \left( \sqrt{\frac{D}{\kappa}} \right)$$

#### 4.2.2. Parallel-beam mode

##### a) Influence of the chemical catalysis on the concentration profiles. The reaction layer

The parallel-beam absorbance profile of the photoactive species R for  $w = 10 \mu\text{m}$  (black points, see Eq.(36)) when a single potential pulse is applied under limiting current conditions is shown in Figure 5 and compared with the theoretical concentration profiles (solid line) calculated from Eqs.(11) and (16) for two different chemical kinetics and for an irreversible ( $K=0$ , see Figs. 5.A and 5.C) or a reversible ( $K=2$ , see Figs. 5.B and 5.D) catalytic reaction. The concentration profile of species O is also plotted (dashed line) as obtained from Eqs. (11) and (16). As can be observed, the faster the catalytic kinetics is, the narrower the perturbed region becomes (indicated on the graphs of Figure 5 as red dotted lines). Hence, a satisfactorily description of the concentration profile via spectroelectrochemistry for fast chemical reactions would require very narrow beam widths (for  $K=0$  and  $0.5 \leq \kappa \leq 5$ ,  $w / \sqrt{D_R / \kappa} \leq 0.6$ , see Section S.II of the Supp. Info.).

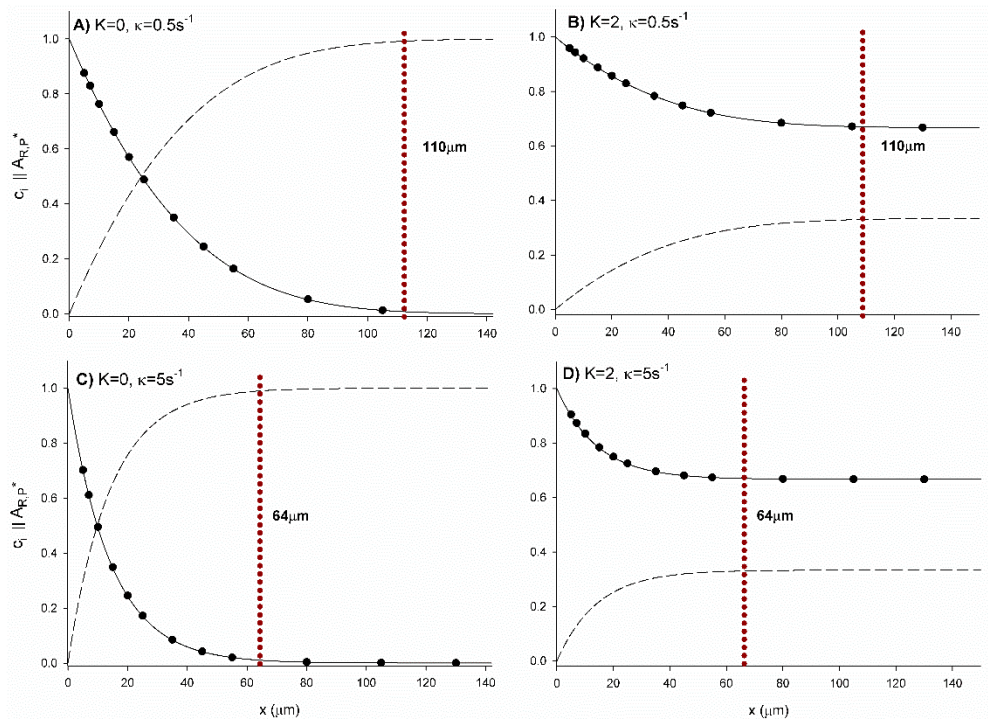


**Figure 5.** Theoretical concentration profiles of the oxidized (dashed lines) and reduced (solid lines) species (Eqs. (11), (15) and (16)) at the end of the first potential pulse under limiting current conditions (for  $t=1\text{s}$ ) and the normalized parallel-beam absorptometric theoretical response of species R (black dots,  $A_{R,P}^* = A_{R,P}^* / (\epsilon_R L_e)$ ) calculated from Eqs. (11), (15), (16) and (28) for  $w = 10 \mu\text{m}$  for two different chemical kinetic and equilibrium constants (indicated on the graphs). Other conditions as in Figure 1.

The agreement observed between the concentration- and  $A_{P,i}$ -profiles in Figure 5 points out that, as in the case of the E mechanism, the parallel-beam absorptometric curves with narrow  $w$ -values can be described accurately by (see S.II of the Supp. Info.):

$$A_{R,P}^{[1],Cat} \approx \varepsilon_R L \left( \frac{c_T}{1+K} \right) \left[ K + Z_1^{Cat} f_{Cat}(x_0 + w/2, t, \kappa) \right] \quad (38)$$

Considering Eq.(38), the value of  $\kappa$  can be estimated as the only adjustable parameter from the theoretical concentration profile given that the  $K$ -value can be calculated very easily from the ratio of the cathodic and anodic limiting current via chronoamperometry:  $I_{L,c}^{CA} / I_{L,a}^{CA} = -1 / K$ .

Getting insight into the experimental profile of function  $\phi(x, t)$  is of great interest because it reflects the magnitude of the disruption of the chemical equilibrium ( $\phi \rightarrow 0$  at the bulk solution), and the thickness of the region where this occurs, the so-called reaction layer.

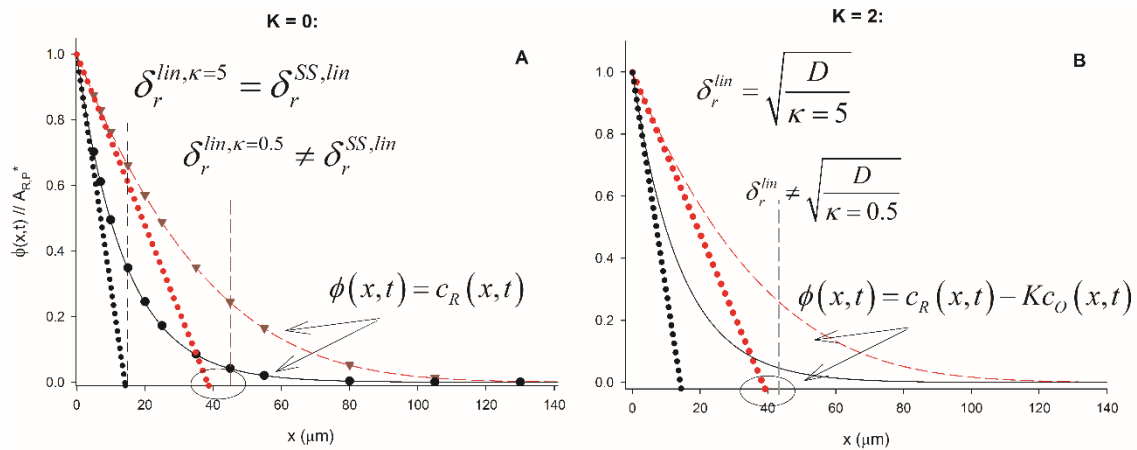


**Figure 6.** Profile of the  $\phi$ -function obtained **A)** directly from the parallel-absorbance profile of species R for  $K=0$  (solid line, Eqs. (11), (15) and (16) and points with Eq. (38)) or **B)** indirectly for  $K=2$  considering also Eqs. (3)-(4). Other conditions as in Figure 5.

In Figure 6, function  $\phi(x, t)$  is plotted for an irreversible (see Fig. 6.A) and a reversible catalytic reaction ( $K=2$ , see Fig. 6.B) and different kinetics (as in Figure 5). As can be expected [15,16],  $\phi(x, t)$  depends on the kinetics of the catalytic reaction in such a way that the faster the catalytic process, the smaller the thickness of the reaction layer.

The value and meaning of the so-called *linear* reaction layer ( $\delta_r^{lin}$ ) compared to the true thickness of the region of non-equilibrium ( $\delta_r^{real}$ ), calculated as the distance from the electrode surface where the value of  $\phi(x,t) \leq 0.01$ , is also examined in Figure 6 where dotted lines show the linearized profile of  $\phi(x,t)$ . In all cases, it can be seen that  $\delta_r^{lin}$  underestimates the real thickness of the reaction layer (between 2.5 and 4.8 times, see section S.III of the Supp. Info.) and the disagreement increases with the chemical kinetics. Also, Figure 6 shows that the  $\delta_r^{lin}$ -value can be calculated accurately as  $\delta_r^{SS,lin} = \sqrt{D/\kappa}$  [15,24,25] for  $\kappa > 1.5 \text{ s}^{-1}$ ; for slower catalytic kinetics, the above expression overestimates the thickness of the linear reaction layer (see section S.III of the Supp. Info.).

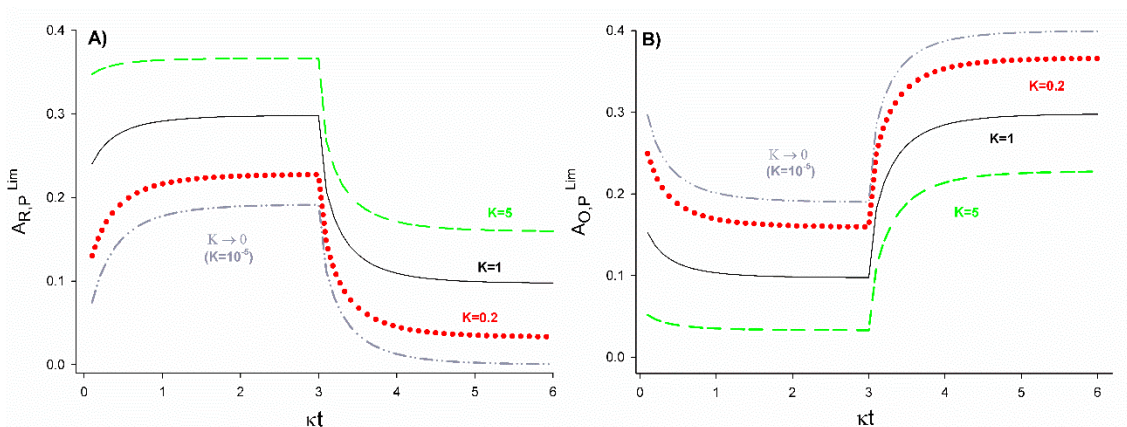
b) Influence of the chemical catalysis on the absorptometric response. Determination of chemical parameters.

Figure 7 shows the influence of the chemical thermodynamics and kinetics of a reversible catalytic mechanism over the chronoabsorptometric response in parallel-beam configuration where it is considered that either species R (Figs. 7.A) or species O (Figs. 7.B) are photoactive and a 50 $\mu\text{m}$  width-beam is employed.

As expected from Eqs. (11) and (16) and from the effects observed in the normal-beam configuration (see Fig.4), the faster the chemical interconversion is (i.e., the larger the  $\kappa t$ -value), the higher the parallel-beam absorptometric response of species R during the first potential step becomes and the opposite for the second potential step. Eventually, time-independent responses are obtained when the interconversion between species R and O is sufficiently fast ( $\kappa t \geq 2$ ). Regarding the influence of the chemical equilibrium constant,  $A_{R,P}$  increases with the K-value, since the bulk concentration of species R increases as the K-value becomes higher.



As shown in Fig. 7.B, the effects of the chemical reaction on the  $A_{O,P}$ -time response are opposite to those observed for the DPC-chronoabsorptometric response of species R.



**Figure 7.** Dimensionless chronoamperometric SEC theoretical responses of **A)** species R and **B)** species O in parallel-beam configuration of a catalytic mechanism as a function of the chemical kinetics ( $\kappa$ ) and thermodynamics ( $K$ ) plotted with Eqs. (11), (15), (16) and (28) and considering  $w=50\mu\text{m}$ . Other conditions as in Figure 3.

Considering the influence of the width-beam (not shown, see Section S.IV of the Supp. Info.), very narrow beams ( $w \lesssim 10\mu\text{m}$ ) are not recommended to study chemical effects since the concentration profiles in the region next to the surface electrode does not differ significantly for different  $\kappa$ -values. Also, very wide beams ( $\gtrsim 200\mu\text{m}$ ) are unsuitable since they lead to poorly sensitive absorptometric responses given the significant contribution of the bulk solution.

In Figure 8 the influence of the chemical equilibrium ( $K$ , see Fig. 8.A) and kinetic constants ( $\kappa$ , Fig. 8.B) on the cyclic voltabsorptometric response of species R is shown. As previously described for the chronoabsorptometric curve, the larger the  $K$ -value or the slower the chemical kinetics are, the higher the voltabsorptometric signal of species R becomes at ‘cathodic’ potentials (see Fig 8.A and 8.B). A similar behavior is observed with  $K$  at ‘anodic’ potentials, while the contrary influence is found with respect to the  $\kappa$ -value.

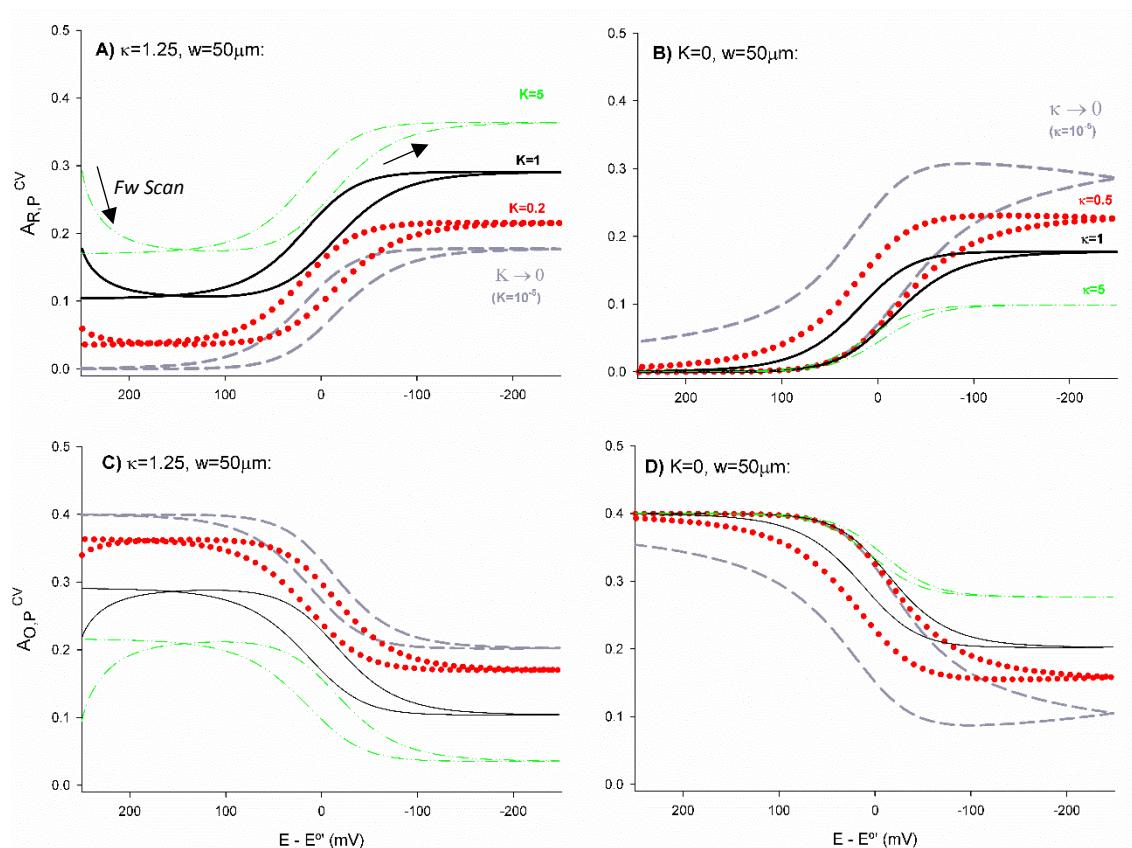


**Figure 8.** Influence of the chemical kinetic constants ( $\kappa$ , see **A**) and of the chemical equilibrium constants ( $K$ , see **B**) over the cyclic voltabsorptometric theoretical responses of species R in parallel arrangement with  $w=50\mu\text{m}$ . The cyclic voltabsorptograms were plotted with Eqs. (11), (15), (16) and (26)-(28). Other conditions as in Figure 3.

Regarding the  $A_{O,P}$ -potential response (see Fig. **8.C** and **8.D**), the opposite behavior is observed since for very fast chemical reactions, the presence of species R in solution becomes almost negligible, being much less significant as the  $K$ -value decreases.

In any case, the voltabsorptometric signal evolve from a transient to a sigmoidal response as the chemical kinetics increases. Also, the forward and backward voltabsorptometric responses intertwine at positive potential for reversible catalytic reactions since species R is initially present at the beginning of the experiment.

## 5. Conclusions

Novel and simple closed-form analytical expressions for the concentration profiles and for the absorptometric response of a (pseudo)first-order reversible catalytic have been deduced based on convenient variable changes prior to the application of the Laplace transform method. They are valid upon the application of any sequence of potential pulses and without any restriction of the chemical rate and equilibrium constants. From the expressions obtained, the influence of the chemical kinetics and thermodynamics on the spectroelectrochemical signal has been analyzed, considering the normal- and the parallel-beam arrangements.

The effect of markedly different diffusion coefficients on the absorptometric signals has also been studied in both working configurations for a simple charge transfer, reporting analytical expressions for any potential perturbation applied. Either for the case of a catalytic mechanism or for a simple charge transfer, simple procedures are proposed to determine the physicochemical parameters of interest from the absorptometric responses.

The signal in the parallel-beam arrangement offers time and spatial valuable information, allowing the monitoring and analysis of the evolution of the concentration profiles. From the determination of the latter, the characteristics of the diffusion and reaction layers can be studied, which are intimately ligated to the properties of the mass transport and of the chemical kinetics and thermodynamics in the system.

### Acknowledgments:

The authors greatly appreciate the financial support provided by the Fundación Séneca de la Región de Murcia (Project 19887/GERM/15) as well as by the Ministerio de Economía y Competitividad (Project CTQ-2015-65243-P). JMGG thanks the Ministerio de Educación, Cultura y Deporte for the fellowship 'Ayuda de Formación de Profesorado Universitario 2015'.

## References

- [1] T. Kuwana, N. Winograd, Spectroelectrochemistry at optically transparent electrodes, in: *Electroanal. Chem. A Ser. Adv.*, Vol. 7, A.J. Bard (Ed.), Marcel Dekker, 1974: pp. 1–78.
- [2] R.G. Compton, D.J. Page, G.R. Sealy, In-situ electrochemical ESR: First-order kinetics and transient signals, *J. Electroanal. Chem. Interfacial Electrochem.* 163 (1984) 65–75. doi:10.1016/S0022-0728(84)80042-X.
- [3] A. Heras, A. Colina, V. Ruiz, J. López-Palacios, UV-visible spectroelectrochemical detection of side-reactions in the hexacyanoferrate(III)/(II) electrode process, *Electroanalysis* 15 (2003) 702–708. doi:10.1002/elan.200390088.
- [4] W. Kaim, J. Fiedler, Spectroelectrochemistry: the best of two worlds, *Chem. Soc. Rev.* 38 (2009) 3373–3382. doi:10.1039/b504286k.
- [5] L. Dunsch, Recent Advances in in situ multi-spectroelectrochemistry, *J. Solid State Electrochem.* 15 (2011) 1631–1646. doi:10.1007/s10008-011-1453-1.
- [6] J.W. Strojek, T. Kuwana, S.W. Feldberg, Spectrochemical-Electrochemical Evaluation of Kinetics Using Optically Transparent Electrodes, *J. Am. Chem. Soc.* 90 (1968) 1353–1355. doi:10.1021/ja01007a045.
- [7] N. Winograd, H.N. Blount, T. Kuwana, Spectroelectrochemical measurement of chemical reaction rates. First-order catalytic processes, *J. Phys. Chem.* 73 (1969) 3456–3462. doi:10.1021/j100844a054.
- [8] J.F. Tyson, T.S. West, Analytical aspects of absorption spectroelectrochemistry at a platinum electrode—II Quantitative basis and study of organic compounds, *Talanta*. 27 (1980) 335–342. doi:10.1016/0039-9140(80)80092-0.
- [9] W. Wanzhi, X. Qingji, Y. Shouzhuo, Theory and application of analytical spectroelectrochemistry with long path length spectroelectrochemical cells, *J. Electroanal. Chem.* 328 (1992) 9–20. doi:10.1016/0022-0728(92)80166-2.
- [10] A. Molina, E. Laborda, J.M. Gómez-Gil, F. Martínez-Ortiz, R.G. Compton, Analytical solutions for the study of homogeneous first-order chemical kinetics via UV-vis spectroelectrochemistry, *J. Electroanal. Chem.* (2017) 1–12. doi:10.1016/j.jelechem.2017.10.031.
- [11] E. Laborda, E.I. Rogers, F. Martínez-Ortiz, J.G. Limon-Petersen, N. V. Rees, A. Molina, R.G. Compton, Reverse Pulse Voltammetry at spherical electrodes: Simultaneous determination of diffusion coefficients and formal potentials. Application to Room Temperature Ionic Liquids, *J. Electroanal. Chem.* 634 (2009) 1–10. doi:10.1016/j.jelechem.2009.06.022.
- [12] A. Martínez, A. Colina, R.A.W. Dryfe, V. Ruiz, Spectroelectrochemistry at the liquid|liquid interface: Parallel beam UV-vis absorption, *Electrochim. Acta.* 54 (2009) 5071–5076. doi:10.1016/j.electacta.2008.12.028.
- [13] R. Pruijsma, R.L. McCreery, Observation of Electrochemical Concentration Profiles by Absorption Spectroelectrochemistry, *Anal. Chem.* 51 (1979) 2253–2257. doi:10.1021/ac50049a045.
- [14] A. Molina, J. González, E. Laborda, R.G. Compton, On the meaning of the diffusion layer thickness for slow electrode reactions, *Phys. Chem. Chem. Phys.* 15 (2013) 2381–2388. doi:10.1039/c2cp43650g.

- [15] A. Molina, I. Morales, Singularities of the catalytic mechanism in its route to the steady state, *J. Electroanal. Chem.* 583 (2005) 193–202. doi:10.1016/j.jelechem.2005.06.003.
- [16] A. Molina, J. González, *Pulse Voltammetry in Physical Electrochemistry and Electroanalysis*, Monographs, Springer International Publishing, Cham, 2016. doi:10.1007/978-3-319-21251-7.
- [17] P. Delahay, G.L. Stiehl, Theory of Catalytic Polarographic Currents, *J. Am. Chem. Soc.* 74 (1952) 3500–3505. doi:10.1021/ja01134a014.
- [18] S.L. Miller, Polarographic Currents from a Combination of Diffusion and Reaction, *J. Am. Chem. Soc.* 74 (1952) 4130–4134. doi:10.1021/ja01136a052.
- [19] A. Molina, Analytical solution corresponding to the  $i/t$  response to a multipotential step for a catalytic mechanism, *J. Electroanal. Chem.* 443 (1998) 163–167. doi:10.1016/S0022-0728(97)00566-4.
- [20] A. Molina, C. Serna, L. Camacho, Conditions of applicability of the superposition principle in potential multipulse techniques: implications in the study of microelectrodes, *J. Electroanal. Chem.* 394 (1995) 1–6. doi:10.1016/0022-0728(95)04005-9.
- [21] A. Molina, C. Serna, F. Martínez-Ortiz, E. Laborda, Double potential step chronoamperometry at spherical electrodes and microelectrodes, *Electrochem. Commun.* 10 (2008) 376–381. doi:10.1016/j.elecom.2007.12.034.
- [22] M.M. Moreno, A. Molina, Further Applications of Cyclic Voltammetry with Spherical Electrodes, *Collect. Czechoslov. Chem. Commun.* 70 (2005) 133–153. doi:10.1135/cccc20050133.
- [23] Y. Xie, S. Dong, Theory of analytical spectroelectrochemistry: reversible reactions, *J. Electroanal. Chem.* 284 (1990) 279–288. doi:10.1016/0022-0728(90)85038-7.
- [24] A. Molina, E. Laborda, J. González, The reaction layer at microdiscs: A cornerstone for the analytical theoretical treatment of homogeneous chemical kinetics at non-uniformly accessible microelectrodes, *Electrochem. Commun.* 71 (2016) 18–22. doi:10.1016/j.elecom.2016.07.006.
- [25] A. Molina, J. González, E. Laborda, R.G. Compton, Analytical theoretical approach to the transient and steady state voltammetric response of reaction mechanisms. Linear diffusion and reaction layers at micro- and submicroelectrodes of arbitrary geometry, *J. Electroanal. Chem.* 782 (2016) 59–66. doi:10.1016/j.jelechem.2016.09.047.